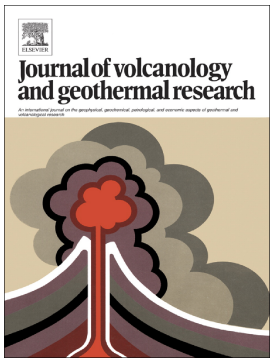

Time scales of olivine storage and transport as revealed by diffusion chronometry at Waitomokia Volcanic Complex, Auckland Volcanic Field, New Zealand

Rosa Didonna, Heather Handley, Helena Albert, Fidel Costa

PII: S0377-0273(24)00086-6

DOI: https://doi.org/10.1016/j.jvolgeores.2024.108094

Reference: VOLGEO 108094

To appear in: *Journal of Volcanology and Geothermal Research*

Received date: 2 December 2023

Revised date: 30 March 2024

Accepted date: 10 May 2024

Please cite this article as: R. Didonna, H. Handley, H. Albert, et al., Time scales of olivine storage and transport as revealed by diffusion chronometry at Waitomokia Volcanic Complex, Auckland Volcanic Field, New Zealand, *Journal of Volcanology and Geothermal Research* (2023), https://doi.org/10.1016/j.jvolgeores.2024.108094

Time scales of olivine storage and transport as revealed by diffusion chronometry at Waitomokia Volcanic Complex, Auckland Volcanic Field, New Zealand.

Rosa Didonna[1,2], Heather Handley[1,3,4], Helena Albert[5], Fidel Costa[6]

[1]*Mineral Resources, Commonwealth Scientific and Industrial Research Organisation (CSIRO), Kensington, WA, Australia*
[2] *School of Natural Sciences, Macquarie University, Sydney, Australia*
[3]*Department of Applied Earth Sciences, Faculty of Geo-Information Science and Earth Observation, University of Twente, The Netherlands*
[4]*School of Earth, Atmosphere and Environment, Monash University, Clayton, Australia*
[5]*Department of Mineralogy, Petrology and Applied Geology, University of Barcelona, Barcelona, Spain*
[6]*Institut de Physique du Globe de Paris, Université Paris Cité, CNRS, Paris, France*

Corresponding author: rosa.didonna@csiro.au

Abstract

Pre-eruptive time scales of magma storage and transport play a critical role in understanding the magmatic processes leading to an eruption. Moreover, these processes still need to be better constrained for mafic volcanic centres in continental intraplate settings as being a source of significant hazards for human populations and infrastructure due to their limited predictability in space and time. We conducted a detailed petrological study to investigate the time scales of olivine storage and transfer throughout the entire evolution of the Waitomokia Volcanic Complex eruption, which encompassed the transition from the initial phreatomagmatic to the final magmatic stage. This volcanic complex is situated within the Auckland Volcanic Field (New Zealand), which was active approximately 250,000 years ago. Olivine crystal textures and compositions were determined from stratigraphically-constrained deposits of the volcanic complex. Olivine crystals are typically skeletal, <300 μm in length, and zoned in forsterite (Fo=100*Mg/[Mg+Fe]; mol%), CaO, MnO and NiO wt.% contents. We classified olivine into three major groups based on their Fo core compositions: (1) normally zoned crystals with high Fo content (Fo>85), (2) crystals with intermediate Fo contents (84-81), and (3) reversely zoned crystals with lower Fo core content (<80). The diffusion profiles of olivine were modelled in the context of a specific magmatic environment linked with changes in thermodynamic variables during storage (temperature, pressure, and oxygen fugacity). We propose that the normally zoned olivine crystals grew in one magmatic environment (ME1), which subsequently intruded into a more evolved environment (ME2), where they interacted and were stored for up to 135 days before the eruption. Moreover,

during the magma ascent to the surface, a second magma mixing event occurred between ME2 and magma within a third magmatic environment (ME3), forming reversely-zoned olivine crystals yielding notably shortener ascent times of approximately a few days. The rocks from the opening phreatomagmatic eruption stage show a larger range in olivine group types compared to the final magmatic activity, where those from the deeper ME1 are more abundant. The short time scales of magma transport obtained in our study, on the order of days to months, should be informative of the warning times that may be encountered between the onset of volcanic unrest and an eruption in the Auckland Volcanic Field.

Keywords: mineral texture, compositional zoning, olivine, Fe-Mg diffusion chronometry, Waitomokia, Auckland Volcanic Field

1. Introduction

The dynamics and time scales of magma storage histories and transport to the surface are periodically investigated through diffusion chronometry in olivine crystals (e.g., Albert et al., 2019, 2020; Kahl et al., 2017; Lynn and Helz, 2022; Sundermeyer et al., 2020). Yet, to date, relatively little research has been carried out on magma ascent processes and timescales in basaltic, continental and intraplate volcanic provinces or fields (Albert et al., 2015; Brenna et al., 2010; Cas et al., 2017; Gutmann, 2002; Jankovics et al., 2019; McGee et al., 2012). Untangling the complexities and dynamics of the pre-eruptive magmatic plumbing system (e.g., magma ascent pathway) is crucial for robust assessments and mitigation of volcanic hazards.

Magma ascent from the mantle source to the surface in basaltic intraplate continental settings is traditionally considered relatively rapid. This interpretation is based on the presence and preservation of mantle xenoliths in erupted volcanic rocks (O'Reilly and Griffin, 2010; Spera, 1984), the lack of significant crystallisation of shallow crustal minerals (e.g. plagioclase), and the dominance of basaltic over evolved rock compositions (McBirney et al., 1987). Moreover, the short time frame between detectable seismicity and eruption for some

historical monogenetic eruptions (Camp et al., 1987; Thorarinsson et al., 1973) points towards minimal storage time in the crust before the eruption. Although intraplate basalts are characterised by small volume, recent investigations (e.g., Kaikohe-Bay of Islands volcanic field and Whangarei volcanic field, New Zealand) revealed how magmas can carry a crystal cargo assembled from various mantle and crustal sources (Coote et al., 2018; Coote and Shane, 2018; Shane and Coote, 2019). Olivine, due to its abundance in basaltic volcanic rocks and frequent compositional zoning, has been widely utilised to investigate these pre-eruptive magmatic processes and ascent (Costa and Chakraborty, 2004; Gordeychik et al., 2018; Hartley et al., 2016; Jankovics et al., 2012; Jollands et al., 2016; Kahl et al., 2015; Lynn and Helz, 2022; Mattioli et al., 2006; Shea et al., 2015; Sundermeyer et al., 2020). Moreover, olivine minerals have revealed complex pre-eruptive magmatic histories in small-volume basaltic volcanic systems (e.g., Albert et al., 2020; Brenna et al., 2018; Coote et al., 2019; Jankovics et al., 2019) involving multiple magma storages during the pathways to the surface. Thus, olivine textures and compositional patterns can be used to model diffusive re-equilibration of geochemical elements (e.g., Ni, CaO) to determine the environment(s) where they grew at specific temperatures, pressure and oxygen fugacity (Caracciolo et al., 2021; Costa and Chakraborty, 2004; Kahl et al., 2011; Kahl et al., 2015).

In this work, we present a detailed petrological study of the juvenile material produced during the various phases (from the initial phreatomagmatic to the final magmatic phase) of the eruptions from the Waitomokia Volcanic Complex, a tuff ring and scoria cone complex in the Auckland Volcanic Field (AVF; Fig. 1). Olivine textures and high-resolution (2-4 μm) compositional zoning profiles were studied to constrain the pre-eruptive magmatic history. We used diffusion models based on the re-equilibration of elements (Mg-Fe, Ca, Ni, Mn) from the olivine core to the rim to obtain the time scales of magmatic processes (e.g., mixing and magma ascent) before eruptions.

Despite over 70 years of quarrying and landscape modification of the volcanic complex, Waitomokia volcano has an excellent continuous exposure preserved of the tuff ring rim deposits, along with the preservation of deposits from the later cone-building stage. This provided a solid stratigraphical framework within which to assess changes in magma

ascent and transport dynamics throughout the monogenetic eruption. The volcanic complex is in the southwest of the AVF, close to critical infrastructure such as the Auckland International Airport and major arterial roads, so understanding ascent dynamics in the area is a source of additional interest for quantifying potential future eruption hazards and risk in the AVF area.

2. Geological background

The AVF in the North Island of New Zealand is an active, continental, intraplate basaltic volcanic field (Fig. 1) containing over 53 volcanic centres spread over an area of ~600 km^2 (Hopkins et al., 2017). The basement under the AVF is inferred to comprise Triassic-to Late Jurassic-aged sedimentary rocks. However, the oldest rocks observed in the outcrop are Miocene-aged, poorly consolidated mudstone and sandstone of the Waitemata Group (Kermode, 1992). The AVF is around 250 km northwest of the active Taupo Volcanic Zone and about 350-400 km west of the active subduction zone of the Pacific Plate beneath the North Island (Sprung et al., 2007). The field has been active over the last ~250 kyrs and has erupted a total estimated volume of approximately 3.4 km^3 of dense rock equivalent (DRE; Allen et al., 1996) with little evidence of any spatiotemporal pattern in eruptions (Cassidy et al., 2007; Hopkins et al., 2017).

A detailed geochemical study by McGee et al. (2013) on AVF volcanic rock compositions revealed variation in source composition within and between volcanic centres in the AVF. Pb isotopes indicated three different source end-members are involved in magma generation within the AVF. Melting likely begins in the deep garnet-bearing asthenosphere. However, melts at individual volcanic centres are mixed with varying proportions from subduction-metasomatized lithosphere, enriched by fluid from subduction episodes and result from variable degrees of partial melting.

Studies of the velocity contrast beneath AVF do not show the presence of a low-velocity zone, as observed in the neighboring Kaikohe-Bay of Islands volcanic field (KBIVF) and Whangarei volcanic field (WVF) in New Zealand (Horspool et al., 2006). The presence

of a low-velocity zone in the mid-crust (10-19 km) may represent a region of partial melt beneath for KBIVF and WVF (Horspool et al., 2006). This significative difference between the two fields and the AVF is still unknow.

Approximately one-third of New Zealand's population lives within the active AVF, corresponding to around 1.66 million people. The last and most voluminous eruption (~2 km^3 DRE) took place at Rangitoto volcano around 500 years ago (Linnell et al., 2016). Many AVF volcanoes show a progression from an initial phreatomagmatic phase with tuff rings and maar craters to a magmatic phase producing scoria cones and lava flows (Agustín-Flores et al., 2014; Allen and Smith, 1994; Hayward et al., 2011; Kereszturi et al., 2013; Molloy et al., 2009). The erupted products in the AVF vary in composition from alkali basalts to nephelinites, with rare sub-alkali basalts (Allen et al., 1996; McGee et al., 2012; McGee and Smith, 2016; Needham et al., 2011). Whole-rock geochemical studies have inferred relatively rapid ascent with minimal stalling or storage of magma in the crust (McGee et al., 2011; McGee et al., 2012; McGee and Smith, 2016; McGee et al., 2013), although some volcanic centres show evidence of crustal assimilation according to Os isotope data (Hopkins et al., 2016). Few mantle-derived xenoliths have been found in the AVF erupted products, with occurrences generally limited to Pupuke (Spargo, 2007) and Onepoto volcanic centres (Searle, 1961) in the north of the AVF (Fig. 1b). Using the whole-rock geochemical compositions for a suite of stratigraphically-constrained volcanic rocks from Crater Hill (south AVF), Smith et al. (2008) ascribed the temporal changes in the chemistry of erupted products to the changing degrees of crystal fractionation from the source to the surface.

To date, few detailed petrological studies (e.g., Brenna et al., 2018) of mineral textures and chemical zoning patterns have been conducted on the AVF volcanic rocks to investigate the crystallisation during magma ascent. A petrographic description of volcanic rocks from several AVF centres was carried out in the 1960s (e.g. Searle, 1961; Searle, 1962). Brenna et al. (2018) measured major, minor, and trace elements, as well as OH profiles, in the rims of xenocrystal olivine from Pupuke. They showed that, at least in the north of the AVF, magma ascent might be characterised by the accumulation and storage of

magma in deep mantle source zones for up to a few years before a very rapid magma ascent (from weeks to less than a month) to the surface.

2.1. Waitomokia Volcanic Complex

The Waitomokia Volcanic Complex is a tuff ring and scoria cone complex located southwest of the AVF (Fig. 1b). In the Maori language, Waitomokia means “water seeping into the ground” (Hayward et al., 2011). The age proposed for Waitomokia volcano is about 20.3ka±0.2ka (Hopkins et al., 2020), during the most active period of the AVF (Hopkins et al, 2017). Unfortunately, due to extensive quarrying and urban development since the 1950s, the three original scoria cones (~30 m high, Fig. 2a) situated within the northeast side of the tuff ring crater are no longer present (Fig. 2b). Although the cones were removed, Cassidy et al. (2007) were able to measure circular gravity and magnetic anomalies in the location of the former cones. Results from their study indicated that a significant subsurface volume of dense and magnetic rock (corresponding to solidified basalt) is still present within the underlying Plio-Pleistocene sediments. However, their results provided no evidence of feeder dykes near the surface (Cassidy et al., 2007). Land use within the complex at the time of fieldwork included a former-quarry, storage yard and a winery (with an annexed vineyard) (Fig. 2b).

Whole-rock compositions of juvenile material at Waitomokia range from basanite to alkali basalt (Griffis, 2013) and lie within the compositional trend (MgO wt.% versus Ni ppm) observed for volcanic rocks from the AVF (see **Fig. 3**).

3. Samples and methods

The volcanic deposits of the Waitomokia Volcanic Complex and the locations of samples used within this study were characterised in detail by Foote et al. (2023). The tuff ring deposits are well exposed in a road cutting in Appendix A1. Deposits from the original scoria cone-building phase were limited due to the prior quarrying of the cones. We examined the remaining outcrops of scoria fall and fluidal spatter-bomb-rich units northwest of the tuff ring

crater. Additionally, an outcrop of coherent lava is exposed in the location of the former westernmost scoria cone. A detailed stratigraphic log of the entire eruption sequence is described by Foote et al. (2023) and a summary of sample's location is illustrated in Supplementary Figure A1.

Based on Foote et al. (2023), an early basal unit composed of tuff and tuff breccia deposits was produced by the initial phreatomagmatic activity and is referred to as *"Initial Phreatomagmatic Stage"* (samples VMA1, VMA7, VMC2, WQE3). The late basal unit (Foote et al., 2023) consisted of lapilli tuff and scoria fall deposits (samples VMC3, VMC4, VMC6 and WQA1) and is referred to in this study as the "*Late Phreatomagmatic Stage*". The magmatic unit (Foote et al., 2023) we refer to in this study as the "*Final Magmatic Stage*" includes juvenile bombs and lava flow deposits (sample WQW1).

3.1. Analytical methods

Optical microscopy was initially used to identify primary mineralogical textures. Backscattered electron (BSE) images of olivine (about 250) and clinopyroxene crystals (about 30 images) were obtained using a Zeiss EVO MA15 scanning electron microscope (SEM) at Macquarie University (Sydney, Australia) using an accelerating voltage of 15 kV. Brightness and contrast were varied to accentuate the textures and visibility of the zoning in minerals.

Quantitative compositional analyses were carried out using a CAMECA SX100 Electron Probe MicroAnalyzer (EPMA) at Macquarie University using an accelerating voltage of 15 kV. The operating conditions were a beam current of 20 nA with a beam diameter of 1 micrometre (µm). The counting time was 10 seconds for Fe, Si, and Al (ka); 20 seconds for Cr and Ca (ka); 30 seconds for Na and P (ka); and 40 seconds for K and Ti (ka). Calibration reference materials are San Carlos olivine (Si, Mg), ilmenite (Ti, Mn, Fe), anorthite (Ca), anorthoclase (Na), Al_2O_3 (Al), chromite (Cr) and fluorapatite (P) for olivine analyses. For clinopyroxene, instead, calibration reference materials are albite (Na, Si), olivine (Mg, Fe), Al_2O_3 (Al), apatite (P), orthoclase (K), casio3 (Ca), tio2 (Ti), chromite (Cr), mngarn (Mn), Ni

(Ni). San Carlos (USNM1111312/444) and Springwater (USNM1111312/444) olivine standards, chromium diopside (AS1120AB; Batbjerg, East Greenland), and diopside (AS1150AB; Wakefield, Quebec, Canada) clinopyroxene standards were analysed to detect accuracy and precision that are function of the absolute abundance of the element (See Appendix B for more details).

We obtained a high-resolution chemical profile of olivine with 2-4 μm sampling space for rim-to-core or rim-to-rim traverses across the compositional gradients on profiles previously selected from the BSE images. Additionally, we acquired approximately 40-point analyses of clinopyroxene. The convolution effect across the sharp boundaries of the chemical changes of the mineral was not considered because it was expected to be <4 μm. Moreover, we did not take into account the phase boundary fluorescence effect (PBF) encountered in EPMA analysis of calcium content in olivine close to grain boundaries with Ca-rich phases such as diopside (Dalton and Lane, 1996). The experimental work of Dalton and Lane (1996) suggests that the increase in olivine calcium concentration due to the PBF when olivine is in contact with diopside is around 0.07 wt.% over a few tens of microns. Hence, the impact of PBF seems limited compared to the CaO increase we observe in the outer rim of olivines (outer 25 micrometres). The increase consistently ranges from ~0.2 to 0.5 CaO wt.% in most crystals. We calculated the Fosterite (Fo) content in olivine following Deer et al. (2013): [Fo= 100 × molar Mg/(Mg+Fe*)] using the total iron Fe* and Mg-number as Mg# = 100 × molar Mg/(Mg+Fe^{*}) for clinopyroxene crystals (for more details, see Appendix B).

Olivine crystallographic orientations were obtained using backscattered electron diffraction (EBSD) on the Zeiss EVO/MA15 SEM with Aztec Software at Macquarie University. Given the significant anisotropy in olivine, these analyses were used to correct for the difference in orientation of the olivine crystallographic directions with the electron microprobe traverses as in Costa and Chakraborty (2004).

4. Diffusion geochronometry modelling

We used the Diffusion Process Analysis (DIPRA) software (Girona and Costa, 2013) to perform the diffusive re-equilibration of Mg-Fe, Mn, Ni And Ca concentrations in olivine. The DIPRA program resolves the diffusion equation numerically, considering the concentration variation (diffusion coefficient dependent) with time at different distances from the core. The program obtains time results through the best fit and the associated error calculation. The model uses the diffusion coefficients of Mg-Fe from Dohmen & Chakraborty (2007a, 2007b), Mn from Ito and Ganguly (2006), Ni from Petry et al. (2004), and Ca from Coogan et al. (2005). The diffusion coefficients are related to the conditions of temperature, pressure, composition, oxygen fugacity, and crystallographic orientation, and the DIPRA program calculates the uncertainty associated with these parameters. To reduce uncertainty in the temperature parameter, we conducted melt-crystallisation modelling utilising alphaMELTS 1.9 software (Gualda and Ghiorso, 2015; Gualda et al., 2012) to estimate the magmatic temperature at which the olivine grew at a range of pressure, water content and melt composition (e.g., Albert et al., 2015) for an oxygen fugacity of NNO oxygen buffer, appropriate for the Auckland Volcanic Field (Brenna et al., 2010; Rowe et al., 2009).

4.1 Initial and boundary conditions

Initial conditions were defined using two main strategies, depending on the shape of the concentration profile being considered. For normally zoned olivine (decreasing Fo concentrations from core to rim), we used a homogeneous initial profile that diffuses due to the gradient variation at the boundary (see Supplementary Figures A4). We used open boundary conditions assuming the re-equilibration of the olivine rim with the more evolved melt at constant composition with time (for more details, see Costa et al., 2008 and Kahl et al., 2011). For olivine profiles that show reverse Fo zoning (increasing concentration from core to rim) or complex zoning, we used non-homogeneous and step-function initial conditions (based on the number of Fo plateaus) with an open boundary between the olivine rim and surrounded melt. For these more complex profiles, we first computed the fit of the

inner part of zoning (at the same initial boundary condition), and later, we used the rim composition that fit the entire profile (see Girona and Costa, 2003).

5. Results

We use the term ‘autocrysts’ to denote a crystal that grew directly from the host magma that transported it to the surface (e.g., Coote et al., 2019) and ‘antecrysts’ for those that originated in the magmatic system but have been inherited from liquids that existed at different times and places (Davidson et al., 2007). We considered ‘xenocrysts’ as crystals derived from elsewhere, such as older cumulate material, country rocks or mantle-derived rocks (Helz, 1987; Welsch et al., 2013). Autocrysts (>300 μm in size), microautocrysts (100-300 μm), and microlites (<100 μm) are described following the definition of Helz (1987), as euhedral or skeletal crystals, with or without inclusions (Fig. 4).

The erupted materials from the Initial Phreatomagmatic Stage consist of juvenile lapilli dominated by skeletal olivine autocrysts up to 5 mm in length (90-95% of the total crystal volume), followed by microautocrysts of clinopyroxene (5-10%) set in a fine-grained groundmass of plagioclase, clinopyroxene, olivine and Fe-Ti oxides. Spherical vesicles are about 100 μm in diameter and sometimes have an elliptical or elongated shape. The samples also contain lithic clasts up to 2-3 mm in size, such as sandstone, silt, and clay. Juvenile bombs are characterised by similar mineralogical assemblage, with autocrysts of olivine (82-90% of the total crystal volume) up to 4 mm in length, microautocrysts of clinopyroxene (9-15%) and oxide (1-3%). The groundmass is vesiculated and made of plagioclase, clinopyroxene, olivine, Fe-Ti oxides and interstitial glass.

The Late Phreatomagmatic Stage deposits are characterised by a similar mineralogical assemblage of the Initial Phreatomagmatic Stage, with autocrysts of olivine (82-90% of the total crystal volume) up to 4 mm in length, microautocrysts of clinopyroxene (9-15%) and Fe-Ti oxide (1-3%). The groundmass is vesiculated and made of plagioclase, clinopyroxene, olivine and Fe-Ti oxides. Lithic clasts up to 2 mm in size, such as sandstone, silt, and clay, are found within the sections analysed.

The Final Magmatic Stage is represented in this study by a coherent deposit of lava at the base of the now-removed scoria cone. This olivine-rich alkali basalt contains olivine autocrysts, the most abundant mineral, reaching a size of up to 3 mm (87% of the total crystal volume). Additionally, microautocrysts of clinopyroxene (10%) and Fe-Ti oxides (3%) are present within a porphyritic groundmass composed of plagioclase, clinopyroxene, olivine, Fe-Ti oxides, and glass.

5.1. Textures and olivine crystal zoning styles

Olivine autocrysts show a wide range in morphology, including euhedral and elongate habits, skeletal or dendritic, and groups of polyhedral autocrysts parallel to each other (Fig. 4). We define the crystal 'core' as the compositionally (relatively) homogeneous interior part of the crystal that is clear, and without inclusions. The olivine core is surrounded by compositionally distinct 'rims' (20-100 μm wide) that are variably zoned (normal or reverse) and are further subdivided within some crystals into 'inner' and 'outer' rims. In all samples, the outermost olivine rims are coated by a few micrometre-thick clinopyroxene rims (Fig. 5). Diverse olivine habits are observed within all eruption stages and appear to be independent of the chemical zoning profile.

Olivine core populations were identified by their compositional plateaus at different Fo contents: high Fo (>85), intermediate Fo (84-81), and low Fo (<80; Fig. 6). The inner rims of most crystals have Fo content of 81-82 (mol %) and outer rim with of lower Fo (75-79). Based on Fo mol% content, CaO wt.% and NiO wt.%, we classified olivine into three groups (Fig. 6 and 7): Group 1 are olivine crystals that are normally zoned, showing a relatively smooth decrease in Fo content from core (>85) to rim (78-80), a CaO content between 0.2-0.4 wt.% and NiO content up to 0.4 wt.% (Fig. 7a). Some olivine rims show an inner plateau (~10 μm long) with Fo contents of 82 mol% (Fig. 7a), similar in composition to Group 2 olivine. Group 2 olivine crystals exhibit normally zoned features, with core Fo content plateaus between 81 and 84 mol% (Fig. 7b) with a relatively smooth transition between core and rim concentrations. Compared to Group 1, olivine crystals from Group 2 have higher

CaO towards the rim (up to 0.5 wt.%) and lower NiO (0.1 wt.%). Olivine crystals in Group 3 display core compositions with relatively lower Fo (78-80) content compared to Groups 1 and 2 and show reverse zoning of the inner rim (Fig. 7). The inner rim displays Fo contents up to ~82 mol%, followed by a decrease in Fo content towards the outer rim (70 mol %). The crystal cores within Group 3 have notably lower CaO (0.1-0.14 wt.%) than the olivine in Groups 1 and 2 and lower NiO (< 0.1 wt.%; Fig. 7c).

Olivine rims show a broader range in CaO content (0.2-0.6 wt.%) compared to the cores (0.1-0.35 wt.%). Fo content is correlated negatively with CaO (Fig. 8a, d) and Mn (c, f) and positively with NiO (Fig 8b, e) for rims, whereas the cores show a vertical trend. Based on CaO-Fo relationships, the rims display three different compositional arrays caused by distinct autocrysts: "high Fo-low CaO" (Fo 80-85, CaO 0.2-0.3 wt%), "intermediate Fo-high CaO" (Fo79-82, CaO 0.3-0.5 wt%), and "low Fo-high CaO" (only for Group 1 olivine; Fo<78, CaO 0.4-0.6 wt%). The transition between "high Fo-low CaO" and "intermediate Fo-high CaO" arrays occurs at -82 with an overlap between the two arrays in Fo content. Fo81

5.2. Clinopyroxene

Clinopyroxene (cpx) occurs as microautocrysts and microlites in the groundmass (Fig. 5). Moreover, cpx of approximately 5-10 μm in length are also found surrounding olivine autocrysts (Fig. 5a), with rims of a few microns in thickness in contact with all olivine crystals (Fig. 5). Cpx compositions are diopside ($Wo_{42-52}En_{30-41}Fs_{10-17}$) and detailed analyses of microautocrysts display oscillatory and sector zonings with cores with Mg# ranging between 70-80 and most of rims Mg# 70 and 72-78 (Fig. 5c).

5.3. Estimation of the temperature and pressure of crystallisation

We first applied the Loucks (1996) thermometer to estimate the co-crystallisation temperature of olivine and clinopyroxene within the magmatic system. However, the results showed that olivine and clinopyroxene were not in chemical equilibrium, which is reflected by clinopyroxene being too Fe-rich to be in equilibrium with the most Fo-rich olivine (Fo 87).

Furthermore, the clinopyroxene-liquid barometer, as proposed by Neave and Putirka (2017), did not demonstrate equilibrium when comparing clinopyroxene and the Mg# in the liquid, assuming a Fe-Mg exchange coefficient of 0.27 ± 0.03 (Appendix A2). Thus, we instead used alphaMELTS 1.9 software (Gualda et al. 2012; Smith and Asimow 2005) to estimate the magmatic temperature of the melt from which the olivine started to crystallise.

We conducted individual modelling runs for each eruptive stage, using the Waitomokia whole rock (Griffis, 2013) as initial composition (VMC2 for the Initial Stage, VMC6 for the Intermediate and WQW1 for the Final Stage; see Appendix C for more details). These runs aimed to model the initial growth conditions, specifically targeting temperatures, pressure, water content and oxygen fugacity (fO_2) close to Ni-NiO oxygen buffer as Rowe et al. (2009) proposed for the Auckland Volcanic Field. Results are showing how the Fo contents in olivine versus temperature is varying in relation with the increase of pressure and water contents (Supplementary Figures_Appendix C). At higher pressure, the Fo content in olivine decrease of about 2 mol% with a temperature increase of about 20°C. Instead, a variation of water content (up to 3 wt%) increase the Fo content in olivine up to 4 mol%.

The conditions characterised by a temperature of 1150±20°C, a pressure of 2 kbar and water content of 1.5-2 wt.% are most representative of the diffusion processing conditions for olivine Group 1 and 2. On the other hand, olivine Group 3 is associated with lower diffusion temperature of about 1120°C, a pressure of 1 kbar and 1 wt% of water content (see Supplementary Figure C1).

5.4. Diffusion modelling results

We defined a magmatic environment (ME) as a melt reservoir where the olivine crystal started to grow. Eventually, olivine crystals moved into another melt reservoir, mingling and mixing with the host reservoir, recording any variations of thermodynamic variables such as temperature, pressure, oxygen fugacity or water content (e.g., Kahl et al., 2011). Thus, we

calculated the magmatic histories recorded by the diffusive re-equilibration of olivine crystals surrounded by a characteristic melt (ME).

Diffusion time results were gained through modelling approximately 22 crystals, indicating a range from a few days to 135 days for olivine Group 1 (Fig. 9). Group 2 olivine crystals exhibited a shorter time of up to 40 days, while Group 3 olivine ranged from a few days up to a month before the eruption was triggered (Fig. 9).

A comprehensive overview of the time scales throughout the evolution of the eruption sequence reveals a gradual reduction in duration, particularly evident during the Final Magmatic Stage with olivine only recorded over 10-15 days (Table 1).

6. Discussion

6.1 Magma ascent processes and pathways at Waitomokia Volcanic Complex

The textural and compositional features of olivine crystals analysed in this study provide essential constraints on magmatic pathways from the source to the surface at the Waitomokia volcanic complex. By examining these characteristics within a well-constrained eruption stratigraphy, we also tracked the potential variations in magma transport, storage, and ascent during the entire eruption as proposed by previous works (e.g., Albert et al., 2020; Jankovics et al., 2019). The identification of distinct compositional plateaus within olivine crystals (Fig. 6**)** provides valuable insights into the various growth environments and melt storage (ME) experienced by these olivine crystals to unravel the dynamics of magmatic processes (e.g., magma recharge, mingling/mixing) and ascent.

The prevalence of euhedral, skeletal and polyhedral olivine habits along with Fo contents of olivine core compositions below 87 mol% suggests that Waitomokia olivine are not derived from the mantle as ultramafic xenocrysts. This is further supported by the lack of observed mantle xenoliths in the volcanic deposits. To date, the presence of large (2-20 mm) anhedral olivine xenocrysts with high forsterite content (Fo ≥ 90) is limited to volcanic rocks in the northern area of the AVF (Brenna et al., 2018; Searle, 1962; Spargo, 2007). Thus, mantle xenoliths and xenocrysts appear to be confined to the North Shore volcanoes,

such as Onepoto and Pupuke (Rodgers et al., 1975; Searle, 1961; Spargo, 2007), suggesting subduction-related origins (Spargo, 2007). Their absence in Waitomokia volcano could imply either that the magma ascent rate was slow compared to the settling and dissolution rates of the mantle xenoliths (e.g., Brearley and Scarfe, 1986; Spera, 1984) or that the melt transfer mechanism physically filters or blocks their ascent.

6.2. Relationship between magmatic environments and olivine groups

The compositional core plateaus observed in olivine crystals (Fig. 6 and 7) suggest that beneath the Waitomokia volcanic complex, there were at least three distinct MEs where olivine cores initiated growth (Fo>85; Fo81-84; Fo< 80). Eventually, the magma from these environments was transferred and mixed within a few days or a month before the eruption. As we assumed progressive crystal growth from core to rim, the final composition at the rim of olivine reflects the most recent environmental conditions or events it encountered.

In this study, olivine Groups are defined by core-rim compositions and compositional zoning patterns. Therefore, Group 1 olivine exhibits cores (Fo>85) associated to the most mafic environment (ME1) and rims formed in a more evolve environment (M2), with 80-82 mol% Fo, akin to the plateau composition of olivine cores from Group 2 olivine, suggesting mixing between M1 and M2. According to alphaMELTS calculations, the conditions of ME2 conditions, where olivine growth and re-equilibration occurred, are characterised by a temperature of 1150±20°C, a pressure of 2 kbar and water content of 1.5-2 wt.%. Additionally, olivine cores observed in Group 3 are linked to the most evolved melt (ME3) with lower Fo and CaO contents (Fo<80; CaO<0.15) and exhibit reverse zoning, with rims reaching up to Fo 82. This indicates a mixing between M2 and ME3 prior the eruption associated with lower diffusion temperature of about 1120°C, a pressure of 1 kbar and 1 wt% of water content for Group 3 olivine. These observations suggests distinct levels of magma storage and mixing for ME2 and M3 at approximately 7Km and 4Km depth, respectively, indicating that the magma did not ascend directly from the mantle source.

Olivine from Group 1 are related to a deeper ME1, but the possible region of melt generation beneath Waitomokia volcano remains unclear.

Other studies related to the AVF have suggested that magma mixing processes may have triggered final melt ascent and eruption, following months to years of storage in the lithospheric mantle. This evidenced by a diffusion study on olivine from Pupuke Maar in the northern area of the AVF (Brenna et al., 2018). The comprehensive geochemical study of McGee et al. (2013) of individual AVF centres found that generated melts are subject to mixing with variable proportions of materials originating from underlying subduction-metasomatized lithosphere enriched by fluids associated with past subduction episodes.

6.3. Variation in the CaO content of olivine and clinopyroxene

The Fo-zoning patterns in olivine and their respective CaO content within Waitomokia volcanic rocks (Fig. 8) provide insights into magma pathways and reactions *en route* to the surface. This relationship is strongly controlled by melt composition (silica activity) and pressure (Stormer Jr, 1973). Olivine from silica-poor alkaline melts (akin to the Waitomokia basanites) are characterised by strong enrichments in calcium content towards olivine rims compared to olivine from more siliceous tholeiitic melts, which show less pronounced enrichment and zonings. CaO content in olivine is expected to decrease with cooling and increase with decreasing pressure. Olivine rim populations at Waitomokia volcano (Fig. 8d) display an increase in CaO at a given Fo content (~Fo 81-82), implying a change in the conditions of crystallisation due to either interaction with a melt with contrasting CaO content or change in, environmental conditions (e.g., temperature or pressure), or both. The significant increase in CaO content in the outermost 25 μm of the rim, coupled with a pronounced decrease in Fo and NiO contents, could be interpreted as crystallisation and decreasing pressure (reflected by higher CaO) and/or decreasing temperature (indicated by lower Fo and NiO). This could be expected to happen during magma's ascent to the surface. The presence of thin Ca-rich clinopyroxene coronas (diopside), measuring just a few micrometres in width, on all the olivine crystals of the Waitomokia samples further suggests

that the melt's CaO content became saturated with Ca-rich clinopyroxene prior the eruption. A petrographic study of the AVF volcanic rocks has similarly observed the presence of these thin clinopyroxenes on olivine rims (Searle, 1962), an indication of the widespread occurrence of the late-stage calcium enrichment in the melt beneath many AVF eruptive centres during the crystallisation process.

Despite their small size, the clinopyroxene microautocrysts show complex oscillatory and sector zoning (Fig. 5). The oscillatory zoning may have resulted from changes in the melt composition due to the mixing processes inferred in this paper and be related to local changes in environmental conditions during growth. These clinopyroxene rims inhibited olivine crystals' re-equilibration with their surrounding melt, resulting in a minimal estimation of the time scales calculated by diffusion modelling. However, studies on clinopyroxene by Welsch et al. (2016) and Ubide et al. (2019) indicate that sector zoning in clinopyroxene appears under near-equilibrium conditions at low degrees of undercooling. Therefore, the euhedral sector-zoned microautocrysts reported in this study, which highlights crystallisation depths corresponding to about 15 km, are likely formed in an environment with little temperature change, contrasting with the skeletal olivines.

Experimental results show that olivine morphology is controlled predominantly by the cooling rate and degree of undercooling (degree of supersaturation) (Donaldson, 1976; Faure et al., 2003). With increased degrees of undercooling, the olivine shape evolves from tablet to skeletal (hopper) to dendritic (swallowtail) (Faure et al., 2003). In the Waitomokia volcanic rocks, the abundant skeletal olivine morphologies (Fig. 4) imply moderate degrees of undercooling and moderate-to-high cooling rates. By contrast, the polyhedral (and euhedral) olivine minerals (e.g., Fig. 4g) suggest a decrease in cooling rate and are associated with a lower growth rate under near-equilibrium conditions. The polyhedral olivine may have formed by cavity-infilling in earlier-formed skeletal olivine (Faure et al., 2003; Welsch et al., 2013). The chemical re-equilibration of Fo in olivine is relatively fast at magmatic temperatures (Chakraborty, 1997; Costa and Chakraborty, 2004; Costa and Dungan, 2005; Dohmen and Chakraborty, 2007). Thus, the preservation of zoning in Fo content in Waitomokia olivines, together with skeletal morphologies, reflects the relatively

fast ascent of magma from source to surface where, at times, melt experienced moderately rapid and significant decreases in temperature after potential events of magma mixing.

7. Implications for the temporal evolution of the Waitomokia volcano

Monogenetic fields are typically considered to be fed by a “simple” magmatic plumbing system, characterised by the direct ascent of magma from the mantle source to the surface (McGee and Smith, 2016). However, recent high-resolution, mineral-scale studies have unveiled the commonality of intricate crustal storage and ascent processes in continental basaltic intraplate volcanoes (Albert et al., 2015; Albert et al., 2016; Brenna et al., 2018; Caracciolo et al., 2021; Jankovics et al., 2019). In particular, studies on monogenetic volcanoes in New Zealand have suggested that magma mixing processes and crustal storage at various levels can be recorded in minerals such as olivine (Coote et al., 2019) or cpx (Shane and Coote, 2018), providing insights into mantle source before crustal interactions occur during their ascent to the surface. Despite studies on velocity contrast are supporting the identification of areas of partial melting, the AVF lacks in low-velocity zones, which is a significant difference compared to the nearby basaltic intraplate areas (KBIVF and WVF). This may imply a more challenging understanding of the melt generation processes beneath Waitomokia volcano due to the absence of information about the source, as also evidenced by the lack of xenoliths transported to the surface. However, an important information available from this study pertains to the highest Fo content in olivine (Fo<87), which are likely already contaminated with the crust during its ascent to the surface. The MEs described in this study are possibly associated with magmatic storage levels (ME2 ~ 7Km and ME3 ~ 4Km), where magma mixing occurred and olivine experienced diffusion processes before leading up to the eruption. This insight is crucial for accurately interpreting the timing of magmatic processes leading to volcanic eruptions could provide a valuable information for mitigating volcanic hazards in densely populated urban areas such as Auckland.

Our findings illustrate the complexity of establishing small-volume, basaltic continental intraplate volcanic systems such as the AVF. Other monogenetic volcanic fields may exhibit similar trends, indicating significant changes in olivine zoning complexity throughout the eruption processes. For instance, at Parícutin volcano in Mexico, olivine zoning patterns varied with stratigraphic position (Albert et al., 2020). At Waitomokia volcano, zoned-olivine crystals representative of Groups 1 to 3 are all found in the eruptive Initial Phreatomagmatic Stage and display a broader range in olivine Fo content (core-rim) than the following stages. However, the transition from the Initial Phreatomagmatic to the Final Magmatic Stage highlights a decrease in the overall textural diversity of olivine groups (1-3), with only Group 1 (the most mafic group) predominant towards the Final Stage of the Waitomokia eruption. This trend finds support in observations from the Fekete-hegy volcanic complex in the Bakony-Balaton Highland Volcanic Field, Eastern Central Europe (Jankovics et al., 2019), where the final magmatic eruptive stage also showed a significant reduction in both the compositional and textural variations among olivine crystals and their spinel inclusions compared to earlier eruption phases.

Our conceptual representation of the sequence of events leading to the eruption is summarised in Fig. 10. During the pre-eruptive stage (Fig. 10a), olivine cores began to form in different environments (ME1-3). Subsequent magma migrations, transports and mixing culminated in the Initial Phreatomagmatic eruption, involving mixing between ME1-ME2, inducing olivine to re-equilibrate over 35-135 days for Group 1 and up to 40 days for Group 2 (Fig. 10b). As magma ME2 ascended towards the surface, it encountered a more evolved magmatic environment (ME3), leading to the formation of reverse-zoned olivine (Group 3) that erupted shortly thereafter, within a month (Fig. 10b). The outer rim of Group 3 olivine exhibits lower Fo and NiO content, but higher CaO content compared the inner rim (Fig. 7c), suggesting formation during the magma's ascent to the surface. Whether or not the volume of eruptive magma in ME3 had been exhausted in the earlier phreatomagmatic phase of the eruption is unclear. However, as the eruption progressed, only magma mixing between ME1 and ME2 continued producing olivine Group 1 and 2. In the Final Magmatic Stage (Fig. 10c), Group 1 is the only dominant olivine group, reaching the surface in a few days.

8. Summary and Conclusions

We have reconstructed the pre-eruptive processes that fed the Waitomokia eruption by combining shape, texture, and compositional zoning patterns in olivine to identify a range of the MEs that were involved from its Initial Phreatomamatic phase to its Final Magmatic activity. Time scales associated with the diffusive re-equilibration of olivine cores in equilibrium with different compositional melts were calculated to identify the time scales of magmatic processes for the critical stages of Waitomokia eruptive history:

1. Three main olivine core groups (1, 2 and 3) were formed in different magmatic environments (ME1, ME2, ME3) that played an essential role in the evolution of the magmatic system.
2. We reconstructed the magmatic histories recorded by the diffusive re-equilibration of olivine in ME2 environment mixed with ME1, showing a range from a few days to 135 days for olivine Group 1 and up to 40 days for some olivine from Group 2. Diffusive time scales calculated for Group 3 and some Group 2 olivine, yielded a time from a few days up to a month, indicative of the magma mixing processes between ME2 and ME3 before the eruption was triggered.
3. During its evolution, the complexity of the magmatic system decreased due to the dominance of the ME1 magma during the Final Magmatic Stage of the eruption. This suggests that the eruptive magma from ME2 and ME3 had been depleted and opened the ascent pathway. The skeletal textures in olivine suggest moderate undercooling and fast magma ascent during transport.
4. Our findings show that continental intraplate basaltic volcanoes, such as those in the AVF volcanic field, can be characterised by magmatic interactions between different magma batches prior to eruption, supporting evidence that magmas are not directly derived from a mantle source.

The short times obtained in this study agree with the previous research on magma ascent timescales for the AVF of Brenna et al. (2018), strengthening our knowledge about this

active volcanic field to support emergency management planning for volcanic hazards in case of future unrest situations.

Acknowledgements

This work was funded by a Macquarie University Research Excellence Scholarship (MQRES) (2015081) associated with an Australian Research Council Discovery Project (DP150100328). We thank Rebecca Griffis for sharing samples and whole-rock data. Lucy McGee is thanked for the helpful discussion during fieldwork in 2016. Ian Weddings and Villa Maria are thanked for granting access to the remaining volcanic outcrops at Waitomokia. We also thank Bruce Hayward for personal communication and historical photos of Waitomokia. H. Albert is a Serra Húnter Lecturer Professor at the University of Barcelona. Warm thanks to Timothy Murphy for his assistance with the lab work. Stefano Caruso and Will Smith for the helpful discussions. We thank two anonymous reviewers for their helpful and constructive reviews and thank Shane Cronin for editorial handling of the manuscript.

Figure captions:

Figure 1: (a) Inset showing the location of the AVF within the North Island, New Zealand. (b) Map of the Auckland Volcanic Field (AVF) and its eruptive centres (adapted from Foote et al. 2022). Deposits from scoria cones, tuff rings and lava deposits are highlighted. The location of the Waitomokia volcano is shown in yellow.

Figure 2: Changes in the geomorphology and land use of the Waitomokia area since the 1950s. (a) The aerial photographs show the presence of three scoria cones (yellow circle) inside the tuff-ring crater (historic photographs; Aviation Whites, 1955); (b) now removed by the quarrying. Present land use within the crater includes a vineyard, a quarry, and a storage yard.

Figure 3: Whole-rock compositions of the studied volcanic centres at the AVF. Variation of MgO (wt.%) vs Ni (ppm) for Motukorea, Mt Eden, Mt Wellington, Pupuke, Purchas Hill, Wiri, Panmure, Outhwaite Park, Puketutu and Orakei (McGee et al. 2013), Rangitoto (Linnell et al. 2016) and Waitomokia volcano (Griffis 2013).

Figure 4: Textural and zoning features of the different olivines found in VMA1, VMC3, WQE3 and WQW1. Olivine crystals show skeletal and dendritic textures with cavities and inclusions (a, c, d, e, f) and groups of polyhedral units of crystals (b, g, h).

Figure 5: (a) Schematic representation of a common olivine crystal with a homogeneous interior composition (core) surrounded by an inner and outer rim (green). The characteristic of all olivine is a rim in contact with a few micrometres (up to 20 μm) of clinopyroxene (cpx; in yellow colour). (b) Backscattered electron image showing detailed sector and oscillatory

zoning in cpx microautocrysts. (c) Mg# number of cpx in contact with olivine and cpx microautocrysts in the groundmass (for rim and core, respectively).

Figure 6: Rim-to-core olivine profile versus Fo (mol %) content from Waitomokia volcano. Plateau core compositions suggest the presence of three olivine groups: one with a core of Fo> 85 and an outer rim of Fo_{82-79}. A second group with Fo 81-84 cores and rims up to Fo 75. And a third group with lower cores Fo<80 and rims up to Fo 73.

Figure 7: Selection of the most representative Fo (mol %), CaO and Ni (wt.%) content profiles. Olivines are classified into three groups based on zoning patterns and Fo composition from rim to core. (a) Group 1: normally zoned olivine with high Fo (>85) core composition, with a significant decrease towards the rim (to Fo~70). (b) Group 2: normally zoned olivine, with intermediate Fo81-84 core and rim up to Fo75. (c) Group 3: reversely zoned olivine, characterised by a core with Fo<80 and an increase in Fo content towards the rim (up to Fo~83-85).

Figure 8: Fo content (mol %) in olivine as a function of CaO (a, d), NiO (b, e) and MnO (c, f) contents for cores and rims, respectively. Different colours are referred to as groups.

Figure 9: Diffusion times calculated for olivine crystals from the three eruption stages at Waitomokia volcanic complex: (a) Initial Phreatomagmatic, (b) Late Phreatomagmatic and (c) Final Magmatic stage and plotted time (in days) from core to the rim of Fo content of olivine that crystallised for each group (1, 2 and 3).

Figure 10: Schematic model showing the evolution of the magmatic plumbing system at Waitomokia Volcanic Complex. (a) Pre-eruption stage, with olivine cores of Groups 1, 2 and 3 growing in different magmatic environments (ME1, 2 and 3, respectively). (b) Interaction between melts from ME1 and ME2, and consequentially ME2 and ME3, likely triggering the Initial Phreatomagmatic eruption. All three olivine groups were found during this stage. (c) Late Phreatomagmatic stage, during which only Groups 1 and 2 were found. (d) In the final magmatic stage, ME1 dominantly feeds the eruption-producing Group 1 olivine.

References

Agustín-Flores, J., Németh, K., Cronin, S.J., Lindsay, J.M., Kereszturi, G., Brand, B.D. and Smith, I.E., 2014. Phreatomagmatic eruptions through unconsolidated coastal plain sequences, Maungataketake, Auckland volcanic field (New Zealand). Journal of Volcanology and Geothermal Research, 276: 46-63.

Albert, H., Costa, F., Di Muro, A., Herrin, J., Métrich, N. and Deloule, E., 2019. Magma interactions, crystal mush formation, timescales, and unrest during caldera collapse and lateral eruption at ocean island basaltic volcanoes (Piton de la Fournaise, La Réunion). Earth and Planetary Science Letters, 515: 187-199.

Albert, H., Costa, F. and Martí, J., 2015. Timing of magmatic processes and unrest associated with mafic historical monogenetic eruptions in Tenerife Island. Journal of Petrology, 56(10): 1945-1966.

Albert, H., Costa, F. and Martí, J., 2016. Years to weeks of seismic unrest and magmatic intrusions precede monogenetic eruptions. Geology, 44(3): 211-214.

Albert, H., Larrea, P., Costa, F., Widom, E. and Siebe, C., 2020. Crystals reveal magma convection and melt transport in dyke-fed eruptions. Scientific Reports, 10(1): 11632.

Allen, S. and Smith, I., 1994. Eruption styles and volcanic hazard in Auckland Volcanic.

Allen, S.R., Bryner, V.F., Smith, I.E. and Ballance, P.F., 1996. Facies analysis of pyroclastic deposits within basaltic tuff-rings of the Auckland volcanic field, New Zealand. New Zealand Journal of Geology and Geophysics, 39(2): 309-327.

Aviation, Whites, 1955. Waitomokia. White Aviation Collection, Alexander Turnbull Library, Auckland, New Zealand.

BREARLEY, M. and SCARFE, C.M., 1986. Dissolution rates of upper mantle minerals in an alkali basalt melt at high pressure: an experimental study and implications for ultramafic xenolith survival. Journal of Petrology, 27(5): 1157-1182.

Brenna, M., Cronin, S.J., Smith, I.E., Sohn, Y.K. and Németh, K., 2010. Mechanisms driving polymagmatic activity at a monogenetic volcano, Udo, Jeju Island, South Korea. Contributions to Mineralogy and Petrology, 160: 931-950.

Brenna, M., Cronin, S.J., Smith, I.E., Tollan, P.M., Scott, J.M., Prior, D.J., Bambery, K. and Ukstins, I.A., 2018. Olivine xenocryst diffusion reveals rapid monogenetic basaltic magma ascent following complex storage at Pupuke Maar, Auckland Volcanic Field, New Zealand. Earth and Planetary Science Letters, 499: 13-22.

Camp, V.E., Hooper, P.R., Roobol, M.J. and White, D., 1987. The Madinah eruption, Saudi Arabia: magma mixing and simultaneous extrusion of three basaltic chemical types. Bulletin of Volcanology, 49: 489-508.

Caracciolo, A., Kahl, M., Bali, E., Guðfinnsson, G.H., Halldórsson, S.A. and Hartley, M.E., 2021. Timescales of crystal mush mobilization in the Bárðarbunga-Veiðivötn volcanic system based on olivine diffusion chronometry. American Mineralogist: Journal of Earth and Planetary Materials, 106(7): 1083-1096.

Cas, R., Van Otterloo, J., Blaikie, T. and Van Den Hove, J., 2017. The dynamics of a very large intra-plate continental basaltic volcanic province, the Newer Volcanics Province, SE Australia, and implications for other provinces. Geological Society, London, Special Publications, 446(1): 123-172.

Cassidy, J., France, S.J. and Locke, C.A., 2007. Gravity and magnetic investigation of maar volcanoes, Auckland volcanic field, New Zealand. Journal of Volcanology and Geothermal Research, 159(1): 153-163.

Chakraborty, S., 1997. Rates and mechanisms of Fe-Mg interdiffusion in olivine at 980°–1300° C. Journal of Geophysical Research: Solid Earth, 102(B6): 12317-12331.

Coogan, L., Hain, A., Stahl, S. and Chakraborty, S., 2005. Experimental determination of the diffusion coefficient for calcium in olivine between 900 C and 1500 C. Geochimica et Cosmochimica Acta, 69(14): 3683-3694.

Coote, A., Shane, P. 2018. Open-system magmatic behaviour beneath monogenetic volcanoes revealed by the geochemistry, texture and thermobarometry of clinopyroxene, Kaikohe-Bay of Islands volcanic field (New Zealand). Journal of volcanology and geothermal research, 368, 51-62. https://doi.org/10.1016/j.jvolgeores.2018.11.006

Coote, A., Shane, P., Stirling, C., Reid, M. 2018. The origin of plagioclase phenocrysts in basalts from continental monogenetic volcanoes of the Kaikohe-Bay of Islands field, New Zealand: implications for magmatic assembly and ascent. Contributions to Mineralogy and Petrology (2018) 173, https://doi.org/10.1007/s00410-018-1440-y

Coote, A., Shane, P., Fu, B. 2019. Olivine phenocryst origins and mantle magma sources for monogenetic basalt volcanoes in northern New Zealand from textural, geochemical and d18O isotope data. Lithos 344-345, 232-246, doi.org/10.1016/j.lithos.2019.06.026

Costa, F. and Chakraborty, S., 2004. Decadal time gaps between mafic intrusion and silicic eruption obtained from chemical zoning patterns in olivine. Earth and Planetary Science Letters, 227(3-4): 517-530.

Costa, F., Dohmen, R. and Chakraborty, S., 2008. Time scales of magmatic processes from modeling the zoning patterns of crystals. Reviews in Mineralogy and Geochemistry, 69(1): 545-594.

Costa, F. and Dungan, M., 2005. Short time scales of magmatic assimilation from diffusion modeling of multiple elements in olivine. Geology, 33(10): 837-840.

Dalton, J.A. and Lane, S.J., 1996. Electron microprobe analysis of Ca in olivine close to grain boundaries: the problem of secondary X-ray fluorescence. American Mineralogist, 81(1-2): 194-201.

Davidson, J., Morgan, D., Charlier, B., Harlou, R. and Hora, J., 2007. Microsampling and isotopic analysis of igneous rocks: implications for the study of magmatic systems. Annu. Rev. Earth Planet. Sci., 35: 273-311.

Deer, W.A., Howie, R.A. and Zussman, J., 2013. An introduction to the rock-forming minerals. Mineralogical Society of Great Britain and Ireland.

Dohmen, R., Becker, H.-W. and Chakraborty, S., 2007. Fe–Mg diffusion in olivine I: experimental determination between 700 and 1,200 C as a function of composition, crystal orientation and oxygen fugacity. Physics and Chemistry of Minerals, 34: 389-407.

Dohmen, R. and Chakraborty, S., 2007. Fe–Mg diffusion in olivine II: point defect chemistry, change of diffusion mechanisms and a model for calculation of diffusion coefficients in natural olivine. Physics and Chemistry of Minerals, 34(6): 409-430.

Donaldson, C.H., 1976. An experimental investigation of olivine morphology. Contributions to Mineralogy and Petrology, 57(2): 187-213.

Droop, G., 1987. A general equation for estimating Fe3+ concentrations in ferromagnesian silicates and oxides from microprobe analyses, using stoichiometric criteria. Mineralogical magazine, 51(361): 431-435.

Faure, F., Trolliard, G., Nicollet, C. and Montel, J.-M., 2003. A developmental model of olivine morphology as a function of the cooling rate and the degree of undercooling. Contributions to Mineralogy and Petrology, 145: 251-263.

Foote, A., Handley, H., Németh, K., Didonna, R., McGee, L., Griffis, R. and Clerke, L., 2023. The role of phreatomagmatism in the formation of complex monogenetic volcanic systems in a low-lying coastal plain. Journal of Volcanology and Geothermal Research, 442: 107899.

Foote, A., Németh, K. and Handley, H., 2022. The interplay between environmental and magmatic conditions in eruption style transitions within a fissure-aligned monogenetic volcanic system of Auckland, New Zealand. Journal of Volcanology and Geothermal Research, 431: 107652.

Girona, T. and Costa, F., 2013. DIPRA: A user-friendly program to model multi-element diffusion in olivine with applications to timescales of magmatic processes. Geochemistry, Geophysics, Geosystems, 14(2): 422-431.

Gordeychik, B., Churikova, T., Kronz, A., Sundermeyer, C., Simakin, A. and Wörner, G., 2018. Growth of, and diffusion in, olivine in ultra-fast ascending basalt magmas from Shiveluch volcano. Scientific Reports, 8(1): 11775.

Griffis, B. 2013. The volcanological and geochemical evolution of Waitomokia Volcano, Auckland Volcanic Field, New Zealand. Honours Thesis, Macquarie University, Sydney, Australia.

Gualda, G.A. and Ghiorso, M.S., 2015. MELTS _ E xcel: AM icrosoft E xcel-based MELTS interface for research and teaching of magma properties and evolution. Geochemistry, Geophysics, Geosystems, 16(1): 315-324.

Gualda, G.A., Ghiorso, M.S., Lemons, R.V. and Carley, T.L., 2012. Rhyolite-MELTS: a modified calibration of MELTS optimized for silica-rich, fluid-bearing magmatic systems. Journal of Petrology, 53(5): 875-890.

Gutmann, J.T., 2002. Strombolian and effusive activity as precursors to phreatomagmatism: eruptive sequence at maars of the Pinacate volcanic field, Sonora, Mexico. Journal of Volcanology and Geothermal Research, 113(1-2): 345-356.

Hartley, M.E., Morgan, D.J., Maclennan, J., Edmonds, M. and Thordarson, T., 2016. Tracking timescales of short-term precursors to large basaltic fissure eruptions through Fe–Mg diffusion in olivine. Earth and Planetary Science Letters, 439: 58-70.

Hayward, B.W., Murdoch, G., Maitland, G. and Jamieson, A., 2011. Volcanoes of Auckland: the essential guide. Auckland University Press Auckland, New Zealand.

Helz, R.T., 1987. Differentiation behavior of Kilauea Iki lava lake, Kilauea Volcano, Hawaii: an overview of past and current work. Geochemical Society, Special Publication, 1: 241-258.

Hopkins, J.L., Timm, C., Millet, M.-A., Poirier, A., Wilson, C.J. and Leonard, G.S., 2016. Os isotopic constraints on crustal contamination in Auckland Volcanic Field basalts, New Zealand. Chemical Geology, 439: 83-97.

Hopkins, J.L., Wilson, C.J., Millet, M.-A., Leonard, G.S., Timm, C., McGee, L.E., Smith, I.E. and Smith, E.G., 2017. Multi-criteria correlation of tephra deposits to source centres applied in the Auckland Volcanic Field, New Zealand. Bulletin of Volcanology, 79: 1-35.

Horspool, N., Savage, M. and Bannister, S., 2006. Implications for intraplate volcanism and back-arc deformation in northwestern New Zealand, from joint inversion of receiver functions and surface waves. Geophysical Journal International, 166(3): 1466-1483.

Ito, M. and Ganguly, J., 2006. Diffusion kinetics of Cr in olivine and 53Mn–53Cr thermochronology of early solar system objects. Geochimica et Cosmochimica Acta, 70(3): 799-809.

Jankovics, M.É., Harangi, S., Kiss, B. and Ntaflos, T., 2012. Open-system evolution of the Füzes-tó alkaline basaltic magma, western Pannonian Basin: constraints from mineral textures and compositions. Lithos, 140: 25-37.

Jankovics, M.É., Sági, T., Astbury, R.L., Petrelli, M., Kiss, B., Ubide, T., Németh, K., Ntaflos, T. and Harangi, S., 2019. Olivine major and trace element compositions coupled with spinel chemistry to unravel the magmatic systems feeding monogenetic basaltic volcanoes. Journal of Volcanology and Geothermal Research, 369: 203-223.

Jollands, M., Hermann, J., O'Neill, H.S.C., Spandler, C. and Padrón-Navarta, J., 2016. Diffusion of Ti and some divalent cations in olivine as a function of temperature, oxygen fugacity, chemical potentials and crystal orientation. Journal of petrology, 57(10): 1983-2010.

Kahl, M., Chakraborty, S., Costa, F. and Pompilio, M., 2011. Dynamic plumbing system beneath volcanoes revealed by kinetic modeling, and the connection to monitoring data: An example from Mt. Etna. Earth and Planetary Science Letters, 308(1-2): 11-22.

Kahl, M., Chakraborty, S., Pompilio, M. and Costa, F., 2015. Constraints on the nature and evolution of the magma plumbing system of Mt. Etna volcano (1991–2008) from a combined thermodynamic and kinetic modelling of the compositional record of minerals. Journal of Petrology, 56(10): 2025-2068.

Kahl, M., Viccaro, M., Ubide, T., Morgan, D.J. and Dingwell, D.B., 2017. A branched magma feeder system during the 1669 eruption of Mt Etna: Evidence from a time-integrated study of zoned olivine phenocryst populations. Journal of Petrology, 58(3): 443-472.

Kereszturi, G., Németh, K., Cronin, S.J., Agustín-Flores, J., Smith, I.E. and Lindsay, J., 2013. A model for calculating eruptive volumes for monogenetic volcanoes—Implication for the Quaternary Auckland Volcanic Field, New Zealand. Journal of Volcanology and Geothermal Research, 266: 16-33.

Kermode, L., 1992. Geology of the Auckland urban area.

Linnell, T., Shane, P., Smith, I., Augustinus, P., Cronin, S., Lindsay, J. and Maas, R., 2016. Long-lived shield volcanism within a monogenetic basaltic field: the conundrum of Rangitoto volcano, New Zealand. Bulletin, 128(7-8): 1160-1172.

Loucks, R.R., 1996. A precise olivine-augite Mg-Fe-exchange geothermometer. Contributions to Mineralogy and Petrology, 125(2-3): 140-150.

Lynn, K.J. and Helz, R.T., 2022. Magma storage and transport timescales for the 1959 Kīlauea Iki eruption and implications for diffusion chronometry studies using time-series samples versus tephra deposits. Bulletin of Volcanology, 85(1): 3.

Mattioli, M., Renzulli, A., Menna, M. and Holm, P.M., 2006. Rapid ascent and contamination of magmas through the thick crust of the CVZ (Andes, Ollagüe region): Evidence from a nearly aphyric high-K andesite with skeletal olivines. Journal of Volcanology and Geothermal Research, 158(1-2): 87-105.

McBirney, A., Taylor, H. and Armstrong, R., 1987. Paricutin re-examined: a classic example of crustal assimilation in calc-alkaline magma. Contributions to Mineralogy and Petrology, 95: 4-20.

McGee, L.E., Beier, C., Smith, I.E. and Turner, S.P., 2011. Dynamics of melting beneath a small-scale basaltic system: a U-Th–Ra study from Rangitoto volcano, Auckland

volcanic field, New Zealand. Contributions to Mineralogy and Petrology, 162: 547-563.

McGee, L.E., Millet, M.-A., Smith, I.E., Németh, K. and Lindsay, J.M., 2012. The inception and progression of melting in a monogenetic eruption: Motukorea Volcano, the Auckland Volcanic Field, New Zealand. Lithos, 155: 360-374.

McGee, L.E. and Smith, I.E., 2016. Interpreting chemical compositions of small scale basaltic systems: a review. Journal of Volcanology and Geothermal Research, 325: 45-60.

McGee, L.E., Smith, I.E., Millet, M.-A., Handley, H.K. and Lindsay, J.M., 2013. Asthenospheric control of melting processes in a monogenetic basaltic system: a case study of the Auckland Volcanic Field, New Zealand. Journal of Petrology, 54(10): 2125-2153.

Molloy, C., Shane, P. and Augustinus, P., 2009. Eruption recurrence rates in a basaltic volcanic field based on tephra layers in maar sediments: implications for hazards in the Auckland volcanic field. Geological Society of America Bulletin, 121(11-12): 1666-1677.

Neave, D.A. and Putirka, K.D., 2017. A new clinopyroxene-liquid barometer, and implications for magma storage pressures under Icelandic rift zones. American Mineralogist, 102(4): 777-794.

Needham, A.J., Lindsay, J., Smith, I., Augustinus, P. and Shane, P., 2011. Sequential eruption of alkaline and sub-alkaline magmas from a small monogenetic volcano in the Auckland Volcanic Field, New Zealand. Journal of Volcanology and Geothermal Research, 201(1-4): 126-142.

O'Reilly, S.Y. and Griffin, W., 2010. Rates of magma ascent: Constraints from mantle-derived xenoliths. Timescales of magmatic processes: From core to atmosphere, 1803799613: 116-124.

Petry, C., Chakraborty, S. and Palme, H., 2004. Experimental determination of Ni diffusion coefficients in olivine and their dependence on temperature, composition, oxygen fugacity, and crystallographic orientation. Geochimica et Cosmochimica Acta, 68(20): 4179-4188.

Rodgers, K., Brothers, R. and Searle, E., 1975. Ultramafic nodules and their host rocks from Auckland, New Zealand. Geological magazine, 112(2): 163-174.

Rowe, M.C., Kent, A.J. and Nielsen, R.L., 2009. Subduction influence on oxygen fugacity and trace and volatile elements in basalts across the Cascade volcanic arc. Journal of Petrology, 50(1): 61-91.

Searle, E., 1961. The petrology of the Auckland basalts. New Zealand journal of geology and geophysics, 4(2): 165-204.

Searle, E., 1962. The volcanoes of Auckland city. New Zealand Journal of Geology and Geophysics, 5(2): 193-227.

Shane, P., Coote, A. 2019. Thermobarometry of Whangarei volcanic field lavas, New Zealand: Constraints on plumbing systems of small monogenetic basalt volcanoes. Journal of volcanology and geothermal research https://doi.org/10.1016/j.jvolgeores.2018.02.013

Shea, T., Lynn, K.J. and Garcia, M.O., 2015. Cracking the olivine zoning code: Distinguishing between crystal growth and diffusion. Geology, 43(10): 935-938.

Smith, I., Blake, S., Wilson, C. and Houghton, B., 2008. Deep-seated fractionation during the rise of a small-volume basalt magma batch: Crater Hill, Auckland, New Zealand. Contributions to Mineralogy and Petrology, 155: 511-527.

Spargo, S.R.W., 2007. The Pupuke volcanic centre: polygenetic magmas in a monogenetic field, University of Auckland.

Spera, F.J., 1984. Carbon dioxide in petrogenesis III: role of volatiles in the ascent of alkaline magma with special reference to xenolith-bearing mafic lavas. Contributions to Mineralogy and Petrology, 88: 217-232.

Sprung, P., Schuth, S., Münker, C. and Hoke, L., 2007. Intraplate volcanism in New Zealand: the role of fossil plume material and variable lithospheric properties. Contributions to Mineralogy and Petrology, 153: 669-687.

Stormer Jr, J.C., 1973. Calcium zoning in olivine and its relationship to silica activity and pressure. Geochimica et Cosmochimica Acta, 37(8): 1815-1821.

Sundermeyer, C., Gätjen, J., Weimann, L. and Wörner, G., 2020. Timescales from magma mixing to eruption in alkaline volcanism in the Eifel volcanic fields, western Germany. Contributions to Mineralogy and Petrology, 175: 1-23.

Thorarinsson, S., SteinthÓRsson, S., Einarsson, T.H., KristmannsdÓTtir, H. and Oskarsson, N., 1973. The Eruption on Heimaey, Iceland. Nature, 241(5389): 372-375.

Ubide, T., Mollo, S., Zhao, J.-x., Nazzari, M. and Scarlato, P., 2019. Sector-zoned clinopyroxene as a recorder of magma history, eruption triggers, and ascent rates. Geochimica et Cosmochimica Acta, 251: 265-283.

Welsch, B., Faure, F., Famin, V., Baronnet, A. and Bachèlery, P., 2013. Dendritic crystallization: A single process for all the textures of olivine in basalts? Journal of Petrology, 54(3): 539-574.

Welsch, B., Hammer, J., Baronnet, A., Jacob, S., Hellebrand, E. and Sinton, J., 2016. Clinopyroxene in postshield Haleakala ankaramite: 2. Texture, compositional zoning and supersaturation in the magma. Contributions to Mineralogy and Petrology, 171: 1-19.

Table 1. Example of selected time scales obtained by modelling the chemical diffusion of Fe-Mg in olivines from Waitomokia volcano. The angles between the crystallographic axes and the traverse are also indicated (α, β, γ).

Stages	Olivine	α	β	γ	Time (days)	Error (-)	Error (+)	Fo rim	Fo core	Boundary composition
Initial Phreatomagmatic	VMA1-01	70.2	21.8	83.7	76	32.69	29.26	81.6	85.7	81.6
	VMA1-06	69.1	54.5	58.8	35	14.9	10.49	81.5	85.1	81.5
	VMA1-07	55.4	42.5	69	90	34.07	31.14	81.4	85.7	81.4
	VMA1-12	84.8	6.4	88.4	135	41.69	38.76	81.7	86.1	81.7
	VMA1-09	38.6	71.2	84.6	8	2.857	2.798	76.7	82.0	76.7
	VMA7_00_1	59.5	15.9	76.5	41	20.75	23.38	80.7	84.8	80.7
	VMA1-14	68	89	23.4	11	6.211	10.74	81.5	78.9	81.5
	VMA7_11_2	17.3	74.6	88.6	17	4.129	8.027	81.2	73.1	81.2
Late Phreatomagmatic	VMC3-01	74.1	38	57	67	15.65	22.43	82.1	86.8	82.1
	VMC6-00	63.2	79.2	29.4	12	5.924	6.791	80.7	85.3	80.7
	WQA1-7	30.1	78.3	62	28	14.34	10.37	81.0	85.0	81.0
	VMC3-14	30.7	74.9	66.7	40	20.25	61.73	81.8	84.1	81.8
	VMC6-02	84.3	54.9	37.4	18	6.979	6.192	82.7	83.5	82.7
	VMC6-08_1	38.3	88.9	51.2	24	5.281	15.97	81.8	83.6	81.8
Final Magmatic	WQW1-c2-2	11.5	89.5	78.3	1	1.217	0.8435	79.4	83.8	79.4
	WQW1-x1	18.5	85.3	69.8	11	3.391	4.5	74.1	85.3	74.1
	WQW1-x1-2	17.1	71.8	88.4	15	4.594	9.278	78.0	84.6	78.0

Author statement

The authors declare they have no competing financial interests.

Declaration of interests

☒The authors declare that they have no known competing financial interests or personal relationships that could have appeared to influence the work reported in this paper.

☐The authors declare the following financial interests/personal relationships which may be considered as potential competing interests:

Highlights:

- Stratigraphically controlled sampling to unveil the magmatic system feeding monogenetic volcanoes within the eruptive sequence.
- The textures and zonings of olivine crystals provided constraints on the storage and pathway to the surface preceding the eruption.
- Diffusion chronometry on olivine related to the entire eruptive sequence.
- Olivine diffusion revealed time scales of magmatic processes ranging from days to a few months.

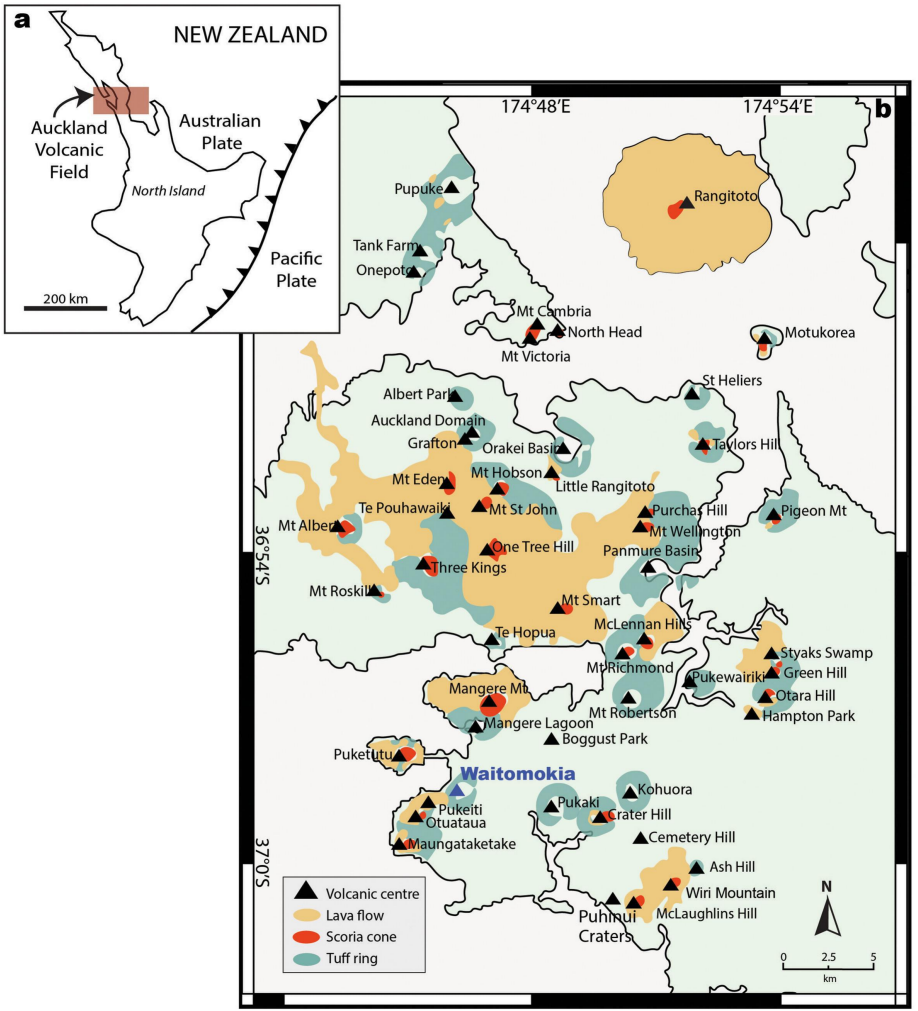
a
NEW ZEALAND
Auckland Volcanic Field
Australian Plate
North Island
Pacific Plate
200 km
b
174°48'E
174°54'E
37°0'S
36°54'S
Pupuke
Rangitoto
Tank Farm
Onepoto
Mt Cambria
North Head
Mt Victoria
Motukorea
St Heliers
Albert Park
Auckland Domain
Grafton
Orakei Basin
Taylors Hill
Mt Eden
Mt Hobson
Little Rangitoto
Te Pouhawaiki
Mt St John
Purchas Hill
Pigeon Mt
Mt Albert
Mt Wellington
One Tree Hill
Panmure Basin
Three Kings
Mt Roskill
Mt Smart
McLennan Hills
Te Hopua
Styaks Swamp
Mt Richmond
Pukewairiki
Green Hill
Mangere Mt
Otara Hill
Mt Robertson
Hampton Park
Mangere Lagoon
Boggust Park
Puketutu
Waitomokia
Kohuora
Pukaki
Crater Hill
Pukeiti
Otuataua
Cemetery Hill
Maungataketake
Ash Hill
Wiri Mountain
McLaughlins Hill
Puhinui Craters
Volcanic centre
Lava flow
Scoria cone
Tuff ring
N
0
2.5
5
km

Figure 1

Figure 2

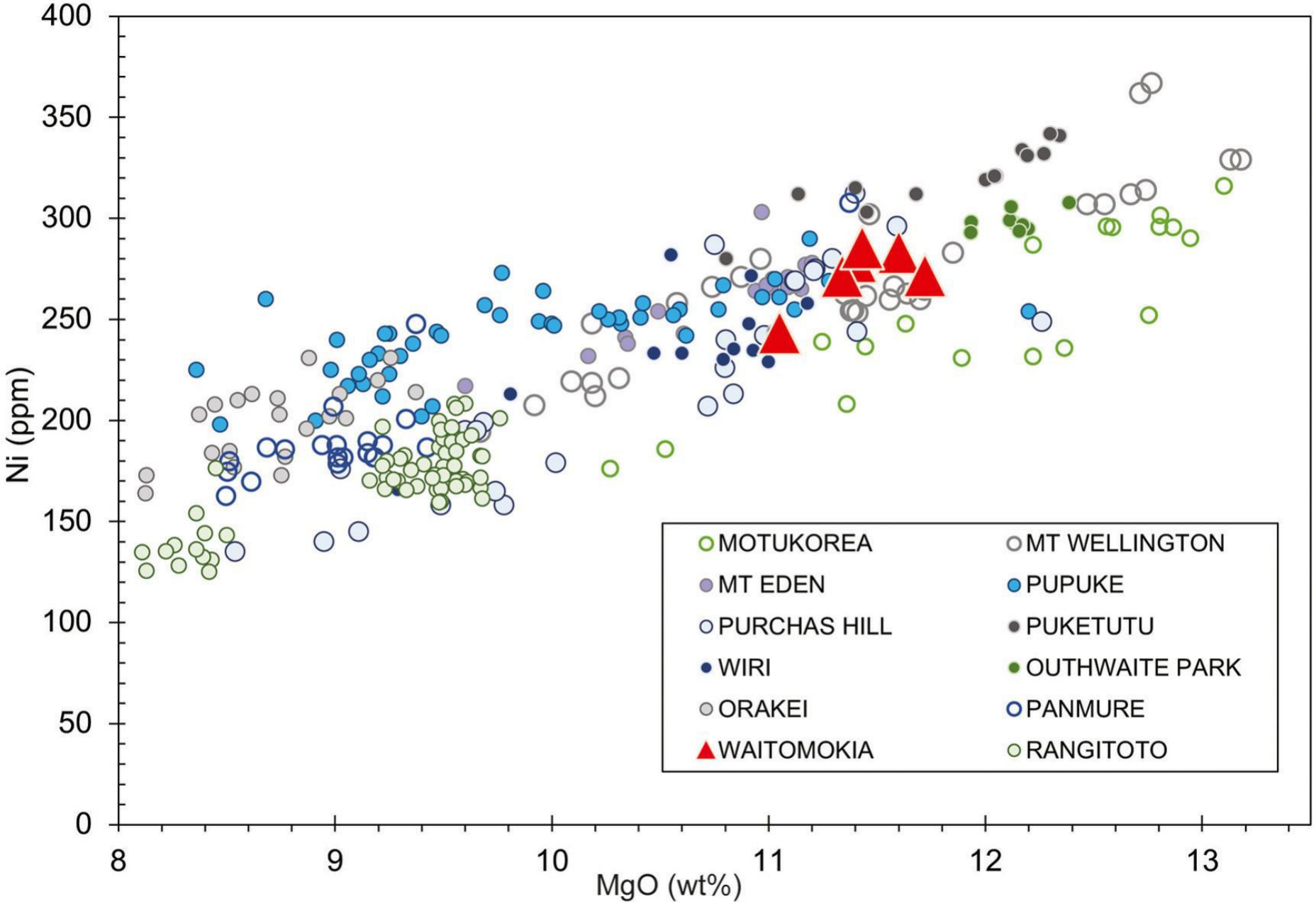
400
350
300
250
200
150
100
50
0
Ni (ppm)
8
9
10
11
12
13
MgO (wt%)
MOTUKOREA
MT WELLINGTON
MT EDEN
PUPUKE
PURCHAS HILL
PUKETUTU
WIRI
OUTHWAITE PARK
ORAKEI
PANMURE
WAITOMOKIA
RANGITOTO

Figure 3

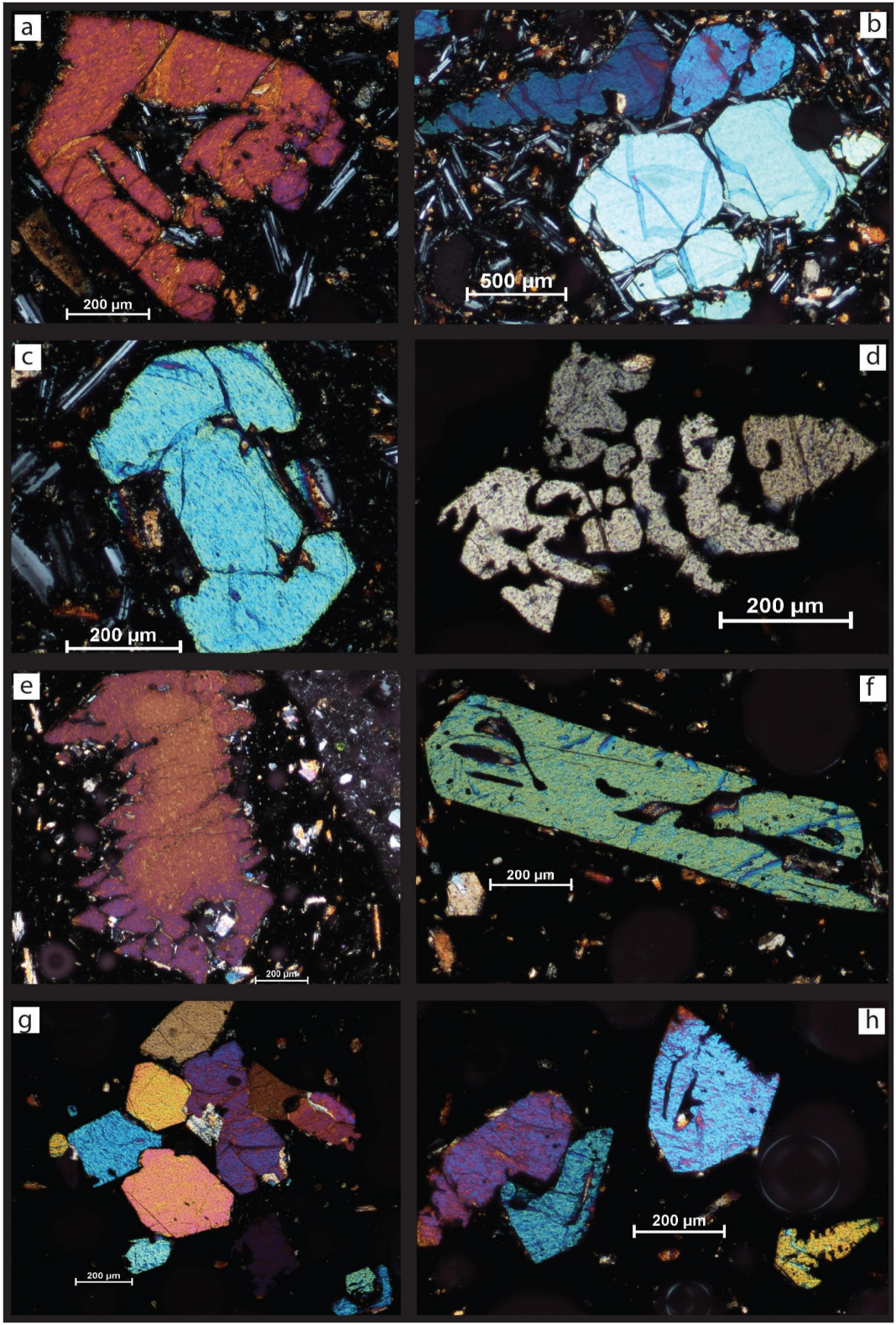

Figure 4

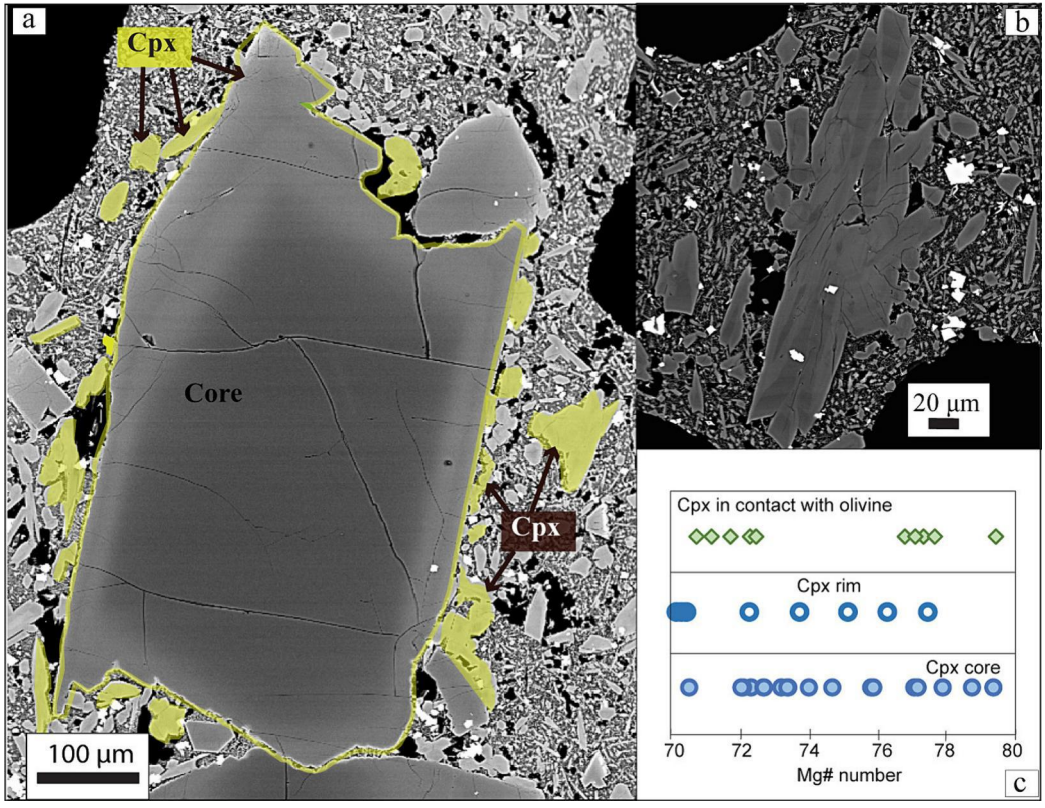
a
Cpx
Core
Cpx
100 µm
b
20 µm
Cpx in contact with olivine
Cpx rim
Cpx core
70
72
74
76
78
80
Mg# number
c

Figure 5

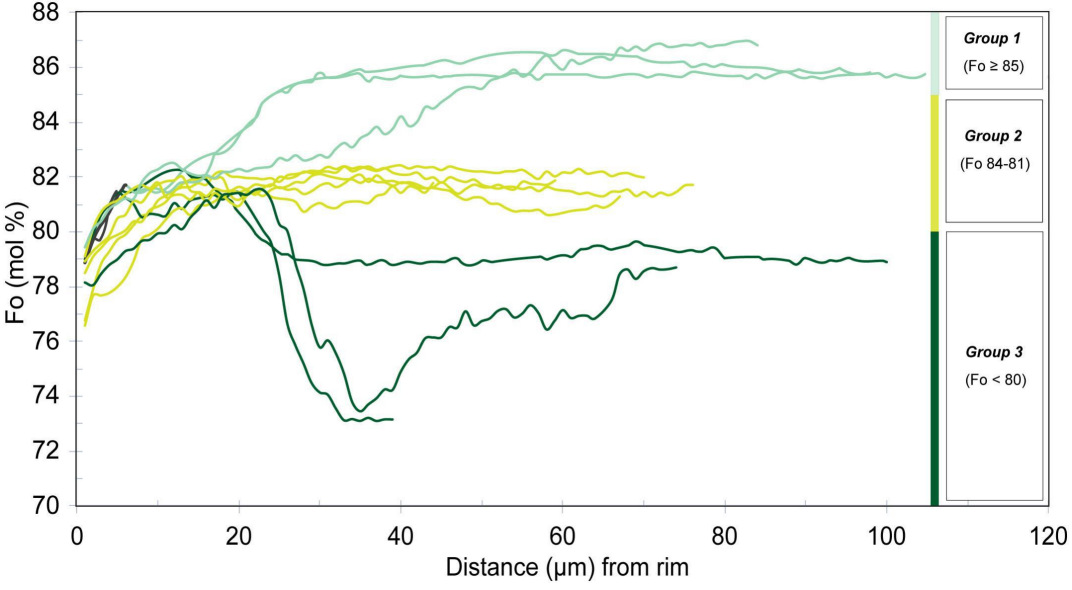
88
86
84
82
80
78
76
74
72
70
Fo (mol %)
0
20
40
60
80
100
120
Distance (µm) from rim
Group 1
(Fo ≥ 85)
Group 2
(Fo 84-81)
Group 3
(Fo < 80)

Figure 6

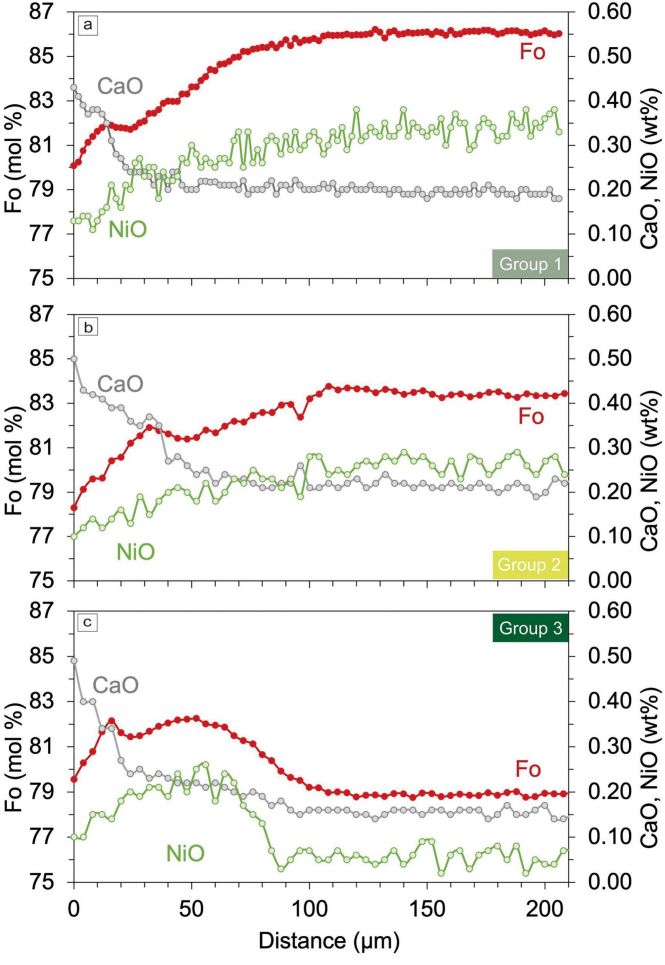
a
b
c
Fo
CaO
NiO
Group 1
Group 2
Group 3
Fo (mol %)
CaO, NiO (wt%)
Distance (μm)
87
85
83
81
79
77
75
0.60
0.50
0.40
0.30
0.20
0.10
0.00
0
50
100
150
200

Figure 7

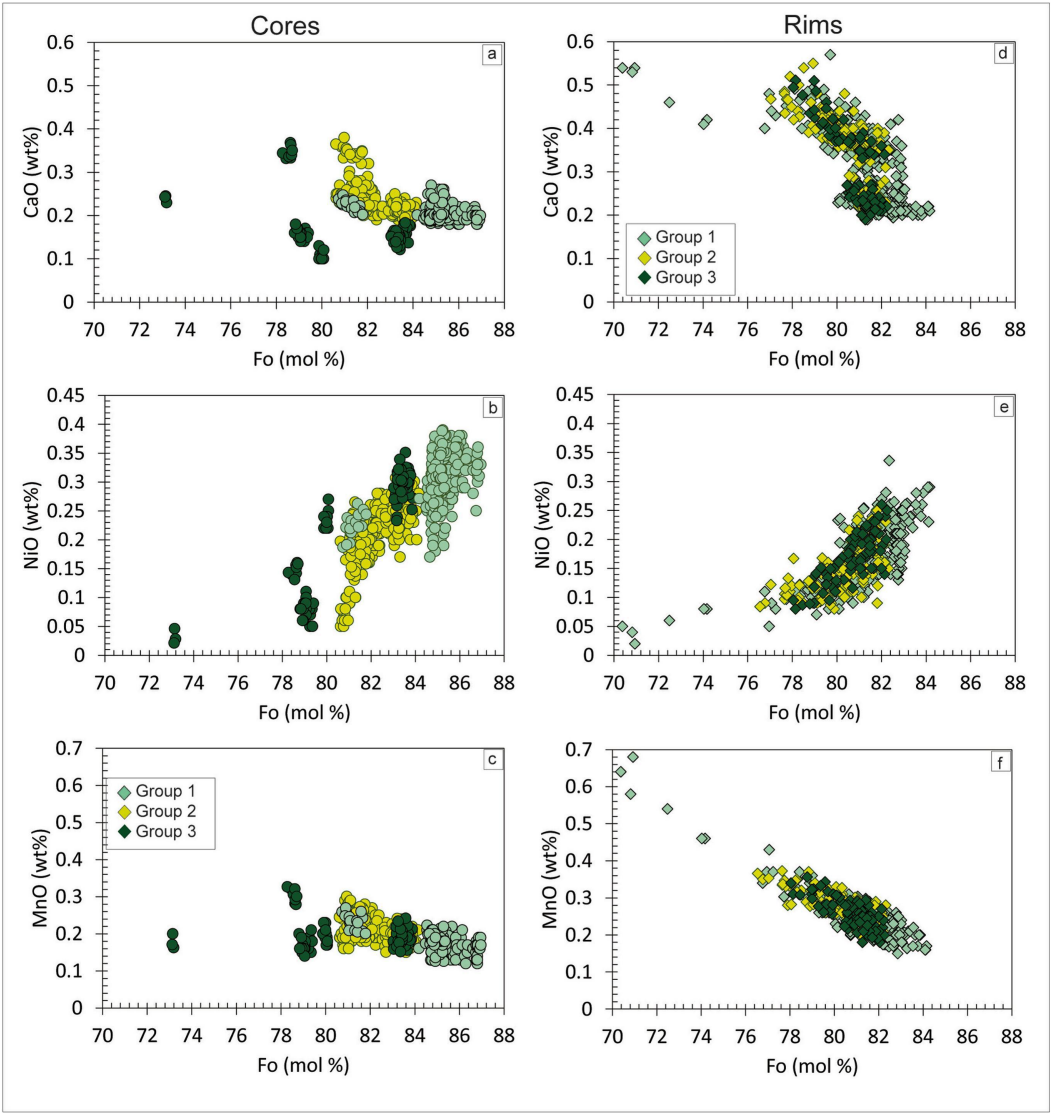
Cores
Rims
a
b
c
d
e
f
CaO (wt%)
NiO (wt%)
MnO (wt%)
Fo (mol %)
Group 1
Group 2
Group 3

Figure 8

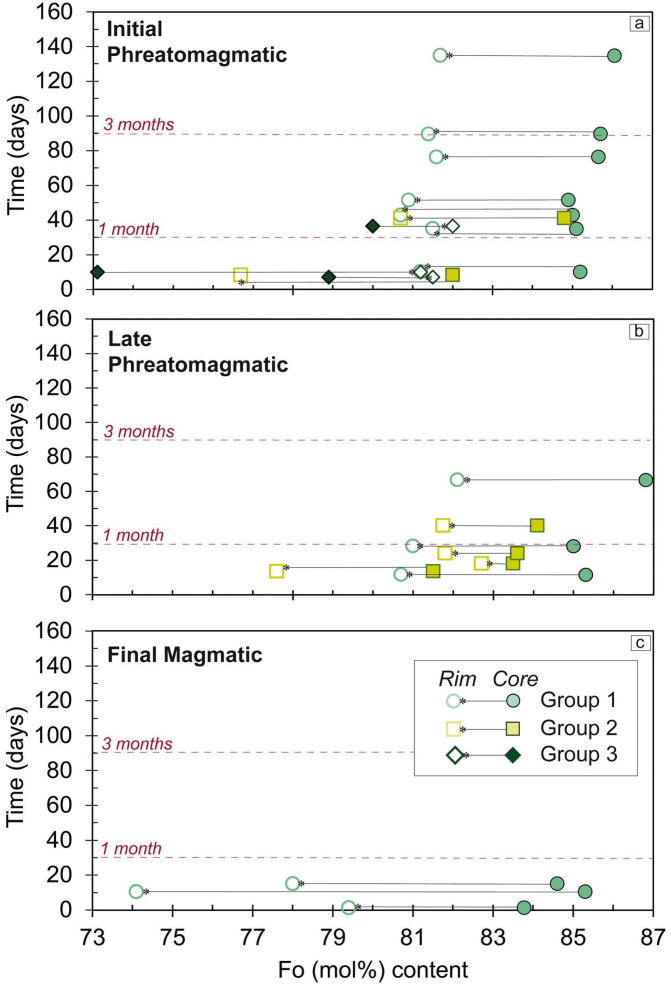
Initial
Phreatomagmatic
a
Late
Phreatomagmatic
b
Final Magmatic
c
Time (days)
3 months
1 month
Rim Core
Group 1
Group 2
Group 3
Fo (mol%) content
0
20
40
60
80
100
120
140
160
73
75
77
79
81
83
85
87

Figure 9

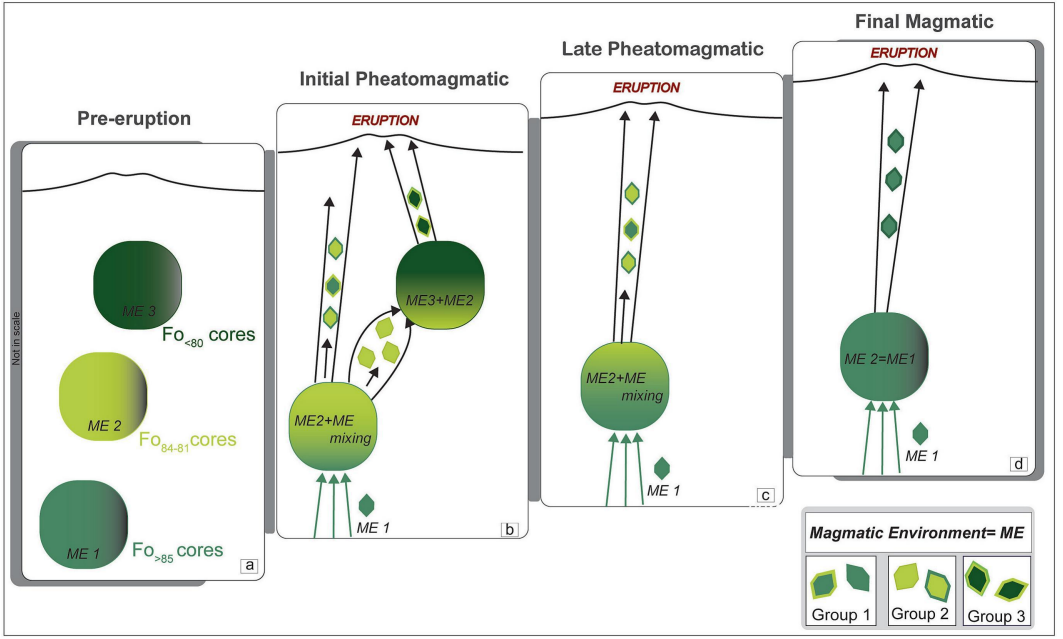
Pre-eruption
Initial Pheatomagmatic
Late Pheatomagmatic
Final Magmatic
ERUPTION
ERUPTION
ERUPTION
ERUPTION
Not in scale
ME 3
Fo<80 cores
ME 2
Fo84-81cores
ME 1
Fo>85 cores
a
ME3+ME2
ME2+ME mixing
ME 1
b
ME2+ME mixing
ME 1
c
ME 2=ME1
ME 1
d
Magmatic Environment= ME
Group 1
Group 2
Group 3

Figure 10